Journal of Alloys and Compounds 516 (2012) 172–178

Contents lists available at SciVerse ScienceDirect

Journal of Alloys and Compounds

journal homepage: www.elsevier.com/locate/jallcom

Free-polymer controlling morphology of α-MoO_3 nanobelts by a facile hydrothermal synthesis, their electrochemistry for hydrogen evolution reactions and optical properties

Hathai Sinaim [a], Dong Jin Ham [b], Jae Sung Lee [b], Anukorn Phuruangrat [c,*], Somchai Thongtem [d,e], Titipun Thongtem [a,e,**]

[a] Department of Chemistry, Faculty of Science, Chiang Mai University, Chiang Mai 50200, Thailand
[b] Eco-friendly Catalysis and Energy Laboratory (NRL), Department of Chemical Engineering, School of Environmental Science and Engineering, Pohang University of Science and Technology, San 31, Hyoja-dong, Pohang 790-784, Republic of Korea
[c] Department of Materials Science and Technology, Faculty of Science, Prince of Songkla University, Hat Yai, Songkhla 90112, Thailand
[d] Department of Physics and Materials Science, Faculty of Science, Chiang Mai University, Chiang Mai 50200, Thailand
[e] Materials Science Research Center, Faculty of Science, Chiang Mai University, Chiang Mai 50200, Thailand

ARTICLE INFO

Article history:
Received 1 January 2011
Received in revised form 4 December 2011
Accepted 11 December 2011
Available online 19 December 2011

Keywords:
Hydrothermal synthesis
α-MoO_3 nanobelts
Hydrogen evolution reactions
Optical properties

ABSTRACT

Orthorhombic molybdenum oxide (α-MoO_3) nanobelts were successfully synthesized by the 100–180 °C and 2–20 h hydrothermal reactions of $(NH_4)_6Mo_7O_{24}{\cdot}4H_2O$ solutions containing 15 ml 2 M acid (HNO_3, H_2SO_4 or HCl) with no surfactant and template adding. These products were characterized by X-ray diffraction (XRD), Fourier transform infrared (FTIR) and Raman spectroscopy, and electron microscopy (EM). In the present research, the product synthesized by the 180 °C and 20 h hydrothermal reaction of the solution containing HNO_3 was α-MoO_3 nanobelts with >10 μm long and <200 nm wide. Electrochemistry for hydrogen evolution reactions (HER) and optical properties of the as-synthesized α-MoO_3 nanobelts were characterized by linear sweep voltammetry (LSV) and Tafel plot, including UV–vis and photoluminescence (PL) spectroscopy. These imply that α-MoO_3 nanobelts show satisfied performance for HER, with the 3.75 eV direct allowed band gap (E_g) due to the charged transition of $O_{2p} \rightarrow Mo_{4d}$, including the emission of 437 nm wavelength at room temperature.

1. Introduction

Over the past decades, scientists and engineers have focused on the fabrication of one-dimensional (1-D) inorganic nanomaterials such as nanowires, nanobelts and nanotubes because these materials exhibit novel chemical and physical properties comparing to their corresponding bulks, owing to the reduced size and large surface area to volume ratio [1].

Among layer inorganic materials, molybdenum oxide (MoO_3) with very interesting catalytic, photochromic and electrochromic properties has been widely used as catalytic material, sensors, smart windows, lubricants and electrochemical storages [1–3]. MoO_3 has two basic structures: the thermodynamically stable orthorhombic MoO_3 (α-type), and the metastable monoclinic MoO_3 (β-type) with ReO_3-type structure. The most important characteristic of α-MoO_3 is its structural anisotropy, considered as a layered structure. Each layer is composed of two sub-layers, formed by corner sharing of octahedrons along the [1 0 0] direction, with edge sharing of octahedrons along the [0 0 1] direction. Alternating stacks of these layered sheets, bound by the van der Waals interaction along the [0 1 0] direction, lead to the formation of α-MoO_3. One might take the benefit of an intrinsic structural anisotropy of α-MoO_3 for tuning its properties by interlayer structural modification and annealing [3,4]. Moreover, α-MoO_3 is a wide band gap (2.6 eV) n-type semiconductor [5], and has been used as a catalyst for hydrogen evolution reaction (HER) [6].

There are a number of reports on the synthesis of 1D MoO_3 nanomaterial which shows a better of both chemical and physical properties than other morphologies. Among them, α-MoO_3 nanorods are promising cathodes in reversible lithium ion batteries. MoO_3 nanobelt films are excellent field emitters. MoO_3 nanorods have been found to be a valuable candidate for use as gas sensors owing to its sensitivity to nitrogen dioxide and anhydrous

* Corresponding author. Tel.: +66 074 288 374; fax: +66 074 288 395.
** Corresponding author at: Department of Chemistry, Faculty of Science, Chiang Mai University, Chiang Mai 50200, Thailand. Tel. +66 053 943 344; fax +66 053 892 277.
E-mail addresses: phuruangrat@hotmail.com (A. Phuruangrat), ttpthongtem@yahoo.com (T. Thongtem).

0925-8388/$ – see front matter © 2011 Elsevier B.V. All rights reserved.
doi:10.1016/j.jallcom.2011.12.024

ammonia, including carbon monoxide and methanol at a working temperature of 200 °C and 40% relative humidity [7].

Nanostructured materials can be synthesized by both physical and chemical methods: solid-state reaction and wet chemical method. Nevertheless, the products obtained from solid-state reactions are irregular morphologies, large particle-sized distribution and non-homogeneous phase. On the other hand, advanced wet chemical method has been succeeded in synthesizing highly purified metal oxides and superconductors with multiple cationic compositions [8]. They include sonochemistry [2], microwave-assisted hydrothermal synthesis [6], spray pyrolysis [9], and hydrothermal reaction [10]. These methods are able to synthesize better crystal quality at lower growth temperature than the solid state route.

In the present research, α-MoO_3 nanostructure was synthesized using a facile hydrothermal process. The influences of different reaction temperatures, holding reaction time and type of acids on phase, morphology and formation mechanism of α-MoO_3 nanostructures were studied. The electrochemistry for hydrogen evolution reaction (HER) and optical properties of the products were also investigated.

2. Experimental

2.1. Synthesis of α-MoO_3 nanobelts

All chemicals with analytical grade, purchased from Fisher Scientific Inc., were used without further purification. First, 0.005 mole ammonium heptamolybdate tetrahydrate ($(NH_4)_6Mo_7O_{24}{\cdot}4H_2O$) was dissolved in 20 ml deionized water with 30 min continuous stirring at room temperature. Second, 15 ml 2 M acid (HNO_3, H_2SO_4 or HCl) was added to this colorless solution, and followed by 30 min stirring. Third, these three mixtures were independently transferred into three lab-made Teflon-lined stainless steel autoclaves to 50 ml capacity. The autoclaves were tightly closed and heated at 100–180 °C for 2–20 h in an electric oven. Finally, light-blue precipitates were synthesized, separated by filtration, washed with distilled water for removal of ionic remains in the final products and followed with ethanol to facilitate water evaporation, and dried at 80 °C in an electric oven for 24 h. Phase, morphology and vibration modes, including electrochemical and optical properties of the products were characterized by a variety of techniques.

2.2. Physical, electrochemical and optical properties of α-MoO_3 nanobelts

The as-synthesized α-MoO_3 nanobelts were characterized by X-ray diffractometer (XRD) on Philips X'Pert MPD using a CuK_α radiation at 45 kV and 35 mA with a scanning rate of 0.04°/s ranging from 10 to 60°. The XRD raw data were interpreted using X'Pert HighScore software. The morphology of the α-MoO_3 nanobelts was investigated by a low vacuum scanning electron microscopy (LV-SEM), JEOL, JSM-5910LV with W as an electron gun. The samples used for LV-SEM were sonicated in ethanol, each of which was subsequently dropped on stubs. Leave them dried in an ambient atmosphere for 24 h, and coat them by gold sputtering. Transmission electron microscopy (TEM) and selected area electron diffraction (SAED) were performed by a JEOL, JEM-2100F at 200 kV. The samples used for TEM analysis were prepared by sonicating of dried products in ethanol for 15 min and depositing 3–5 drops of the suspensions onto carbon foils supported on copper grids. FTIR spectra were recorded on Perkin Elmer Spectrum RX FTIR spectrophotometer with KBr as a diluting agent and operated in the range of 400–4000 cm^{-1} with the resolution of 4 cm^{-1}. Raman spectroscopy, T64000 HORIBA JOBIN YVON, was operated using 30 mW He–Ne laser with 632.8 nm wavelength.

The hydrogen evolution reaction (HER) was tested by a Princeton Applied Research (PAR) for linear sweep potential from −0.20 to 0.20 V (vs RHE) with a scanning rate of 50 mV s^{-1}, using a glassy carbon, Pt wire and Ag/AgCl (3 M NaCl) as working, counter and reference electrodes, respectively, in 1 M H_2SO_4 solution as electrolyte. Working electrode was prepared as explained in the previous reports [6,11].

Absorption property of the as-synthesized α-MoO_3 nanobelts was studied in colloid solutions on Perkin Elmer, Lambda-25 UV–visible (UV–vis) spectrometer in 250–800 nm wavelength range. Photoluminescent (PL) property was investigated by LS50B Perkin Elmer fluorescence spectrophotometer using 337 nm excitation wavelength at room temperature. Each sample for photonic testing was prepared by dissolving 0.02 g product in 100 ml ethanol and followed by 10 min sonication.

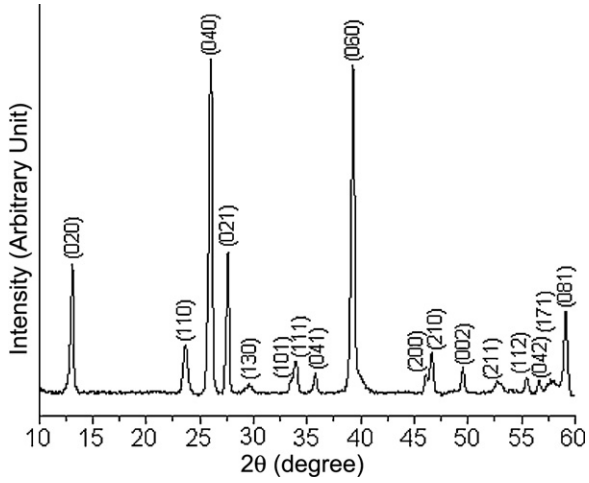

Fig. 1. XRD pattern of α-MoO_3 nanostructure synthesized by hydrothermal reaction at 180 °C for 20 h.

3. Results and discussion

3.1. Characterization of α-MoO_3 nanobelts

The as-synthesized MoO_3 product was characterized by XRD in order to identify the phase and structure of the product. Fig. 1 shows XRD pattern of the MoO_3 product synthesized by hydrothermal method under 180 °C for 20 h using $(NH_4)_6Mo_7O_{24}{\cdot}4H_2O$ as molybdenum source and followed by 15 ml 2 M HNO_3 addition. All the diffraction peaks of the product were identified to correspond with orthorhombic MoO_3 (α-MoO_3) of the JCPDS No. 05-0508 [12]. It should be noted that the intensities in the family (0 k 0) planes with k = 2, 4, and 6 were higher than those of the standard which revealed a layered crystal structure or a highly anisotropic growth of the oxide [10,13]. Considering MoO_3, it is an orthorhombic structure, composed of highly distorted MoO_6 octahedrons which are interconnected with the edges in the [0 0 1] direction and interlinked with the corners in the [1 0 0] direction, leading to a so called double-layer planar structure. Each of these double layers is zigzag bonded together by the van der Waals force to make the product appear as stratified structure [14,15]. Therefore, the increasing in the intensities of the (0 2 0), (0 4 0) and (0 6 0) planes implies that the unit cells of layer-structured α-MoO_3 crystal are highly anisotropic growth along the b axis.

Fig. 2 shows the low and high magnification SEM images of α-MoO_3. At low magnification (Fig. 2a), the product is completely uniform α-MoO_3 nanobelts with no detection of any other morphologies. Their lengths are >10 μm, and their widths are <200 nm. The α-MoO_3 nanobelts hydrothermally synthesized by other researchers are compared in Table 1. The present research is at an advantage in synthesizing these α-MoO_3 nanobelts without using any polymers in controlling the structure. The high magnification SEM image (Fig. 2b) shows that the surfaces of α-MoO_3 nanobelts are smooth and even. A typical nanobelt is 100–120 nm thick.

FTIR spectrum (Fig. 3a) shows the vibrational interaction between molybdenum and oxygen atoms of α-MoO_3 nanobelts. The sharp band at 996 cm^{-1} is assigned as the terminal oxygen symmetric stretching vibration of Mo═O belonging to the layered structured α-MoO_3 phase [14,16,17]. The vibration band at 882 cm^{-1} corresponds to the bridge oxygen asymmetric stretching vibration of Mo—O—Mo [13,14,16,17], and at 570 cm^{-1} to the symmetric stretching vibration of O atoms linked to three Mo atoms [13,14,16].

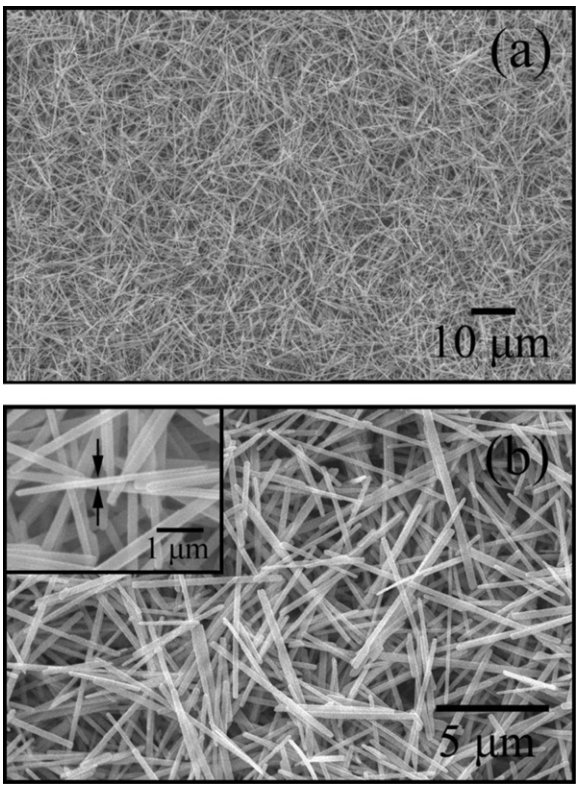

Fig. 2. SEM images at (a) low and (b) high magnifications of α-MoO_3 nanobelts synthesized by hydrothermal reaction at 180 °C for 20 h.

The α-MoO_3 is a layer structure with ABA stacking, which contains edge- and corner-linked octahedrons. The Mo^{6+} ions occupy in octahedral interstices within the lattice of O^{2-} ions. Layered α-MoO_3 structure is composed of one Mo atom and three nonequivalent types of O atoms, namely, O_1, O_2, and O_3. The Mo—O_1 is the shortest bond with 1.67 Å apart. In the *c* axis, there are two equal Mo—O_2 bonds with 1.95 Å long, and the third bond is in the *b* axis with 2.33 Å long. Along the *a* axis, there are two Mo—O_3 bonds with 1.73 and 2.23 Å long [18]. Group theory predicted the following irreducible representation at the center (Γ) of Brillouin zone. Optical vibrational modes of molybdenum oxide with $D_{2h}{}^{16}$ (Pbnm) space group are given as follows.

$$\Gamma = 8A_g + 8B_{1g} + 4B_{2g} + 4B_{3g} + 4A_u + 3B_{1u} + 7B_{2u} + 7B_{3u} \quad (1)$$

where A_g, B_{1g}, B_{2g}, and B_{3g} are Raman-active modes. A_u is an inactive mode, and B_{1u}, B_{2u} and B_{3u} are infrared-active modes [18,19]. The Raman spectrum of α-MoO_3 operated using 632.8 nm wavelength of He–Ne laser at 50–1100 cm^{-1} is shown in Fig. 3b. Roughly speaking, the Raman spectrum of α-MoO_3 was classified into stretching, deformation and lattice modes at 1000–600, 400–200, and below 200 cm^{-1}, respectively [18,20]. The peak at 159 cm^{-1} is the A_g/B_{1g} mode, corresponding to the δ $(O_2Mo_2)_n$ polyhedrons along with the chain axis. Its intensity was strongly increased by the polarization along the *c* axis. The peaks at 82, 98, 116, and 127 cm^{-1} were specified as the A_g, B_{2g}, B_{2g} and B_{3g}, corresponding to the T_a, T_a, T_c and T_c translation of rigid MoO_4 chain modes, respectively. Between 400 and 200 cm^{-1} vibrations are the 245 (B_{3g}, δ O_2—Mo—O_2 scissoring), 292 (B_{3g}, δ O_1=Mo=O_1 wagging), 338 (A_g/B_{1g}, δ O_3—Mo—O_3 bending), and 379 cm^{-1} (B_{1g}, δ O_2=Mo=O_2 scissoring) peaks. The peak at 471 cm^{-1} is the A_g mode which corresponds to the ν_{as} Mo—O_2—Mo stretching and bending vibration. The 664 cm^{-1} peak is the B_{2g}/B_{3g} mode, corresponding to the ν_{as} Mo—O_2—Mo stretching. Those at 816 and 992 cm^{-1} are the A_g modes. They are specified as the ν_s Mo—O_3—Mo stretching of which bonding aligns along the *a* axis, and ν_{as} Mo=O_1 stretching of which bonding aligns along the *b* axis [18–24]. Different Raman vibration modes of the present α-MoO_3 nanobelts and those of other reports are compared in Table 2.

TEM image of α-MoO_3 (Fig. 4a) shows uniform nanobelts with 100–200 nm wide and several μm long. Their surfaces are very smooth and even. The selected area electron diffraction (SAED) patterns (Fig. 4b–d) were recorded perpendicular to the growth direction of the three nanobelts of Fig. 4a. They appear as bright spots of electron diffraction patterns which indicate the single crystalline nanobelts with high crystallinity. All SAED patterns were indexed to correspond with the (0 0 1), (1 0 1) and (1 0 0) planes with the electron beams in the [0 1 0], [0 1 0], and [0–10] directions of the individual α-MoO_3 nanobelts as compared to those of the JCPDS standard No. 05-0508 [12]. They were suggested that the product was α-MoO_3 nanobelts growing along the [0 0 1] direction [10]. The α-MoO_3 nanobelt structure model (inset of Fig. 4a) grows along the *c* axis, with the ±(1 0 0) top and bottom, ±(0 1 0) side, and ±(0 0 1) end surfaces [10]. In general, α-MoO_3 is composed of distorted MoO_6 octahedrons with sharing corners along the [1 0 0] direction (*a*-axis), and zigzag edges along the [0 0 1] direction (*c*-axis) to form layers. Each of the layers is bound together by the weak van der Waals attraction along the *b*-axis to form the pronounced nanomaterial with large surface area to volume ratio [16,19].

In contrast, the interaction along the *c* axis is strong covalent bond, implying that more energy was released during their growth along the [0 0 1] direction. The energy release was in favor with the growth of α-MoO_3 unit cells along the *b* axis. The XRD peaks of the (0 *k* 0) planes were higher than those of the corresponding standard, since the (0 1 0) plane retained in the final product, as the consequence of fast growing rate [6,10].

The formation mechanism of α-MoO_3 nanobelts from isopolymolybdate $(Mo_7O_{24})^{6-}$ anions under hydrothermal treatment was reported by Lou and Zeng [4] as follows.

$$Mo_7O_{24}{}^{6-} + 6H^+ \rightarrow 7MoO_3 + 3H_2O \quad (2)$$

The $Mo_7O_{24}{}^{6-}$ anions were obtained by dissolving of $(NH_4)_6Mo_7O_{24}{\cdot}4H_2O$ as starting material in a solution containing HNO_3. The overall equilibrium would shift the hydrothermal reaction to the right, although several intermediate steps may proceed. Thus other compounds/phases may exist. However, Xia et al. [25] suggested the growth of 1-D α-MoO_3 nanostructure by electroneutral and dehydration reactions as follows.

$$Mo_7O_{24}{}^{6-} + 6H^+ + 11H_2O \rightarrow 7MoO_3{\cdot}2H_2O \quad (3)$$

Table 1
The 1D α-MoO_3 nanostructure synthesized by hydrothermal reactions.

Researchers	Mo source	Polymer	Temperature (°C)	Time (h)	Morphology	Length (μm)	Width (nm)
Wang et al. [10]	$(NH_4)_6Mo_7O_{24}{\cdot}4H_2O$	CTAB	180	20	Nanobelts	>5	100–200
Reddy et al. [13]	$(NH_4)_6Mo_7O_{24}{\cdot}4H_2O$	PVP	180	360	Nanorods	6	5–100
Reddy et al. [16]	$(NH_4)_6Mo_7O_{24}{\cdot}4H_2O$	PEG	180	96	Nanobelts	1–5	100–600
Mohan et al. [17]	$(NH_4)_6Mo_7O_{24}{\cdot}4H_2O$	PEG	180	48	Nanobelts	<0.32	70–180
Ours	$(NH_4)_6Mo_7O_{24}{\cdot}4H_2O$	Free	180	20	Nanobelts	>10	<200

CTAB, cetyltrimethyl ammonium bromide; PVP, polyvinylpyrrolidone; PEG, polyethylene glycol.

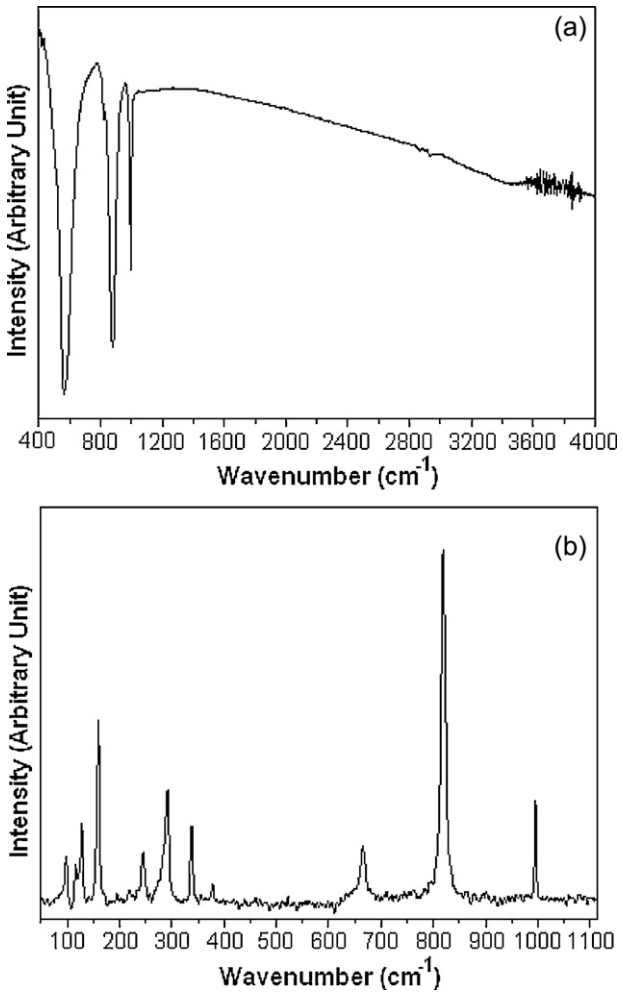

Fig. 3. (a) FTIR and (b) Raman spectra of α-MoO_3 nanobelts synthesized by hydrothermal reaction at 180 °C for 20 h.

At high temperature, water was released by two steps as follows.

$$MoO_3{\cdot}2H_2O \rightarrow \alpha\text{-}MoO_3{\cdot}H_2O + H_2O \quad (4)$$

$$\alpha\text{-}MoO_3{\cdot}H_2O \rightarrow \alpha\text{-}MoO_3 + H_2O \quad (5)$$

The crystal structure of $MoO_3{\cdot}2H_2O$ is monoclinic symmetry and does not display any one-dimensional chain structure. α-$MoO_3{\cdot}H_2O$ exhibits Mo—O—Mo chains running along the [0 0 1] direction. There is the maximum intensity of one-dimensional growth due to the presence of two different sorts of chains along the *a* and *c* axes of orthorhombic α-MoO_3 [25].

3.2. The effect of reaction temperature, holding time and type of acids on the formation of α-MoO_3 nanobelts

The effect of reaction temperature, holding time and type of acids was studied during the formation of α-MoO_3 nanobelts. Figs. S1 and S2 of the Supporting Information show the XRD patterns and SEM images of α-MoO_3 nanobelts, which were synthesized by hydrothermal reactions at 100–180 °C for 20 h. XRD analysis proved that the product at 100 °C for 20 h was composed of mixed phase of hexagonal MoO_3 (h-MoO_3) and orthorhombic α-MoO_3, corresponding to the JCPDS No. 21-0569 for h-MoO_3, and 05-0508 for orthorhombic α-MoO_3 [12]. The h-MoO_3 phase became lessened when the reaction hydrothermal temperature was increased. Pure α-MoO_3 was synthesized at 140 °C and above, with no detection of any other impurities. The α-MoO_3 nanobelts were agglomerated as nanobelt bundles at 100–160 °C for 20 h. They were separated into individual uniform nanobelts at 180 °C for 20 h. Figs. S3 and S4 of the Supporting Information show the XRD patterns and SEM images of α-MoO_3 nanobelts synthesized by the hydrothermal reactions at a constant temperature of 180 °C for 2–20 h. When the reaction time was decreased from 20 h to 5 h, the product remained as pure α-MoO_3 phase. Upon reducing the length of time to 2 h, the mixture of h-MoO_3 and α-MoO_3 as minor and major phases was detected. At this stage (180 °C, 2 h), the agglomerated bundle of nanobelts was synthesized. For longer time (5–10 h), individual of α-MoO_3 nanobelts was synthesized, but composed of a mixture of nano- and micro-belts. At 180 °C for 20 h, uniform α-MoO_3 nanobelts were synthesized and detected.

When either HCl or H_2SO_4 instead of HNO_3 was used, the XRD patterns (Fig. S5 of the Supporting Information) remained the same, excluding intensities of the diffraction peaks. The XRD patterns also corresponded to the pure phase of α-MoO_3, but all intensities of the diffraction peaks of α-MoO_3 for using of HCl and H_2SO_4 became lessened – lowering the degree of crystallinity. The products synthesized in the HCl and H_2SO_4 acidic solutions, shown by SEM images (Fig. S6 of the Supporting Information), are short agglomerated α-MoO_3 nanobelts. These proved that the reaction hydrothermal temperature, holding reaction time and type of acids are the key factors used to control pure phase and uniform α-MoO_3 nanobelts. In general, the nanomaterials with high crystallinity

Table 2
Raman vibration modes of α-MoO_3 nanostructures.

Raman vibration modes	Assignment	Wavenumber (cm^{-1})					
		Ours	Ref. [18]	Ref. [21]	Ref. [22]	Ref. [23]	Ref. [24]
A_g	T_a Translation of rigid MoO_4 chain (T_a)	82	–	89	82	82	83
B_{2g}	T_a Translation of rigid MoO_4 chain (T_a)	98	–	100	–	98	98
B_{2g}	T_c Translation of rigid MoO_4 chain (T_c)	116	116	116	115	114	116
B_{3g}	T_c Translation of rigid MoO_4 chain (T_c)	127	130	129	129	128	128
A_g/B_{1g}	$\delta\,(O_2Mo_2)_n$	159	157	159	158	157	156
B_{2g}	$\delta\,O_2$—Mo—O_2 scissoring	196	198	197	198	197	198
A_g	$\delta\,O_2$—Mo—O_2 scissoring	218	217	216	216	216	218
B_{3g}	$\delta\,O_2$—Mo—O_2 scissoring	245	246	247	246	244	246
B_{2g}	$\delta\,O_1$=Mo=O_1 wagging	283	284	285	284	282	286
B_{3g}	$\delta\,O_1$=Mo=O_1 wagging	292	291	293	–	–	291
A_g/B_{1g}	$\delta\,O_3$—Mo—O_3 bending	338	338	334	336	336	338
A_g	$\delta\,O_2$=Mo=O_2 scissoring	365	365	366	365	365	366
B_{1g}	$\delta\,O_2$=Mo=O_2 scissoring	379	378	376	379	377	380
A_g	ν_{as} Mo—O_2—Mo bending	471	471	473	–	469	472
B_{2g}/B_{3g}	ν_{as} Mo—O_2—Mo stretching	664	667	667	666	666	666
A_g	ν_s Mo—O_3—Mo stretching	816	817	823	819	818	820
A_g	ν_{as} Mo=O_1 stretching	992	996	996	996	994	996

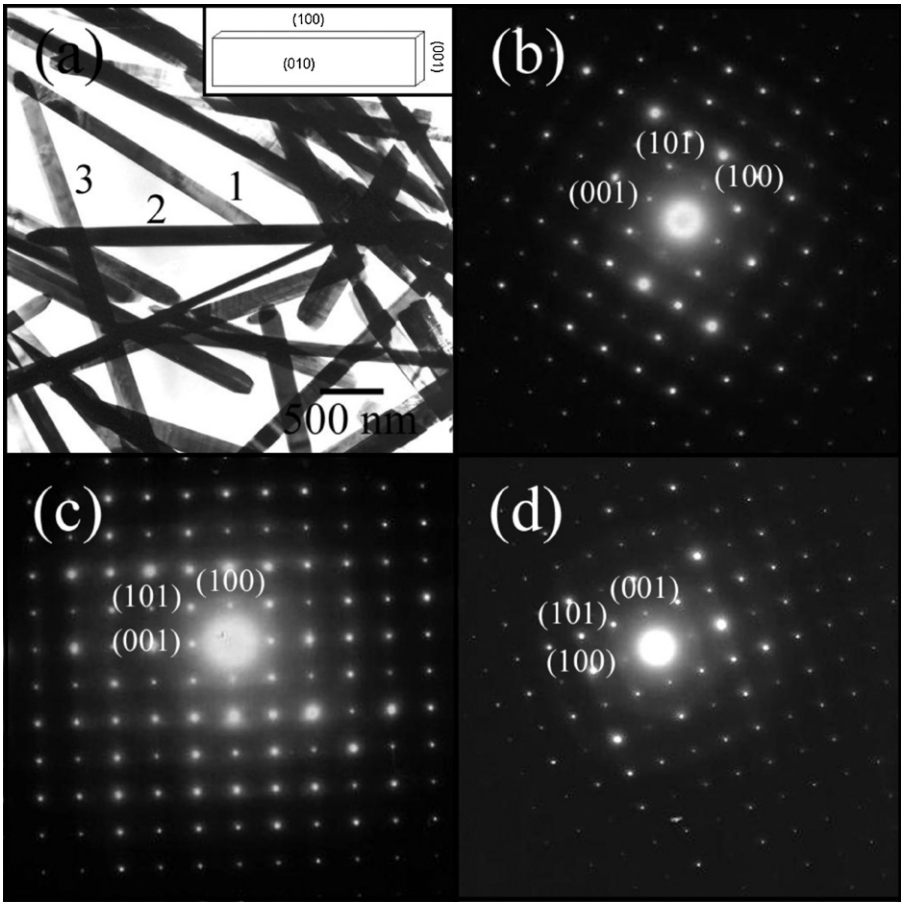

Fig. 4. (a) TEM image and structure model (inset) of α-MoO_3 nanobelts synthesized by hydrothermal reaction at 180 °C for 20 h, and (b–d) SAED patterns on the 1, 2 and 3 nanobelts of (a).

and uniform morphology have the potential to improve the electrochemical and photoluminescent properties. Therefore, the best condition for the synthesis of uniform α-MoO_3 nanobelts with high crystallinity in this research is the 180 °C and 20 h hydrothermal processing of the solution containing 15 ml 2 M HNO_3.

3.3. Electrochemical property of α-MoO_3 nanobelts

α-MoO_3 is a material with tunnel structure for using in electrochromic applications, constituted by $[MoO_6]^{6-}$ octahedrons with sharing edges and corners, resulting in zigzag chains and unique layers binding along the [0 1 0] direction. Consider three phases of MoO_3, monoclinic (β-MoO_3) is metastable. At 140 °C and above, h-MoO_3 (hexagonal) would transformed into orthorhombic α-MoO_3 – the most thermodynamically stable phase [10,14]. Smaller ions such as H^+ and Li^+ can be intercalated in its layer structure [16,17,26–28]. The hydrogen evolution reaction (HER) in 1 M H_2SO_4 with α-MoO_3 nanobelts as a catalyst can be explained as follows [11].

$$xH^+ + xe^- + MoO_3 \rightarrow H_xMoO_3 \quad \text{cathodic reaction} \tag{6}$$

$$H_xMoO_3 \rightarrow 0.5xH_2 + MoO_3 \quad \text{anodic reaction} \tag{7}$$

where x is the stoichiometric parameter which varied between 0 and 1. When a voltage (cathodic reaction) was applied, H^+ ions migrated in the layered $[MoO_6]^{6-}$ octahedrons along the (0 1 0) plane of α-MoO_3, with electron trapping on some Mo^{6+}, forming Mo^{5+}. Coloration was attributed to the intervalence charged transition between Mo^{6+} and the newly formed Mo^{5+}. The intercalated

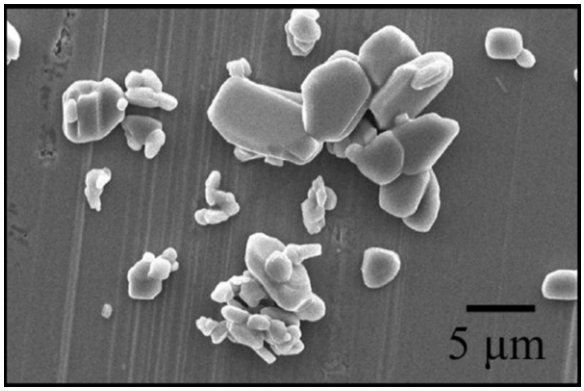

Fig. 5. SEM image of commercial MoO_3 microparticles.

H_xMoO_3 is known as the molybdenum bronze [28]. At the anodic reaction, it led to the oxidation of Mo(V) with the evolution of H_2 gas [6,11]. The HER of α-MoO_3 nanobelts was investigated by linear sweep voltammetry (LSV) and Tafel plot comparing to the commercial MoO_3 microparticles with the particle size of 2–5 μm (Fig. 5).

Fig. 6 shows the LSV curves of pure glassy carbon electrode (black/top), commercial MoO_3 microparticles (blue/middle), and α-MoO_3 nanobelts (green/bottom). The pure glassy carbon electrode shows no actively electrochemical reaction. When the surfaces of glassy carbon electrodes were coated by commercial MoO_3 microparticles

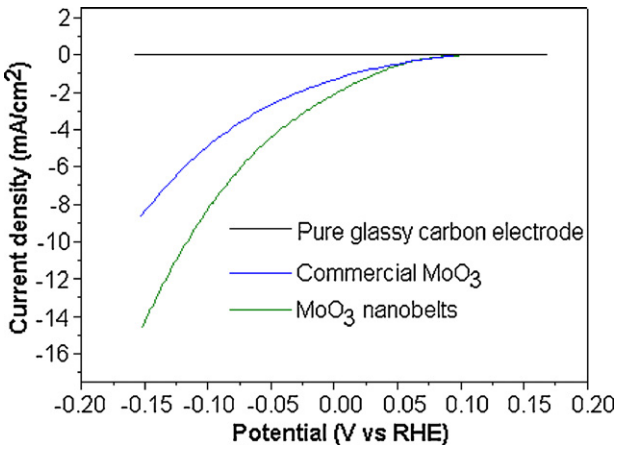

Fig. 6. LSV curves of HER testing for pure glassy carbon, and carbon electrodes coated with α-MoO_3 nanobelts and commercial MoO_3 microparticles.

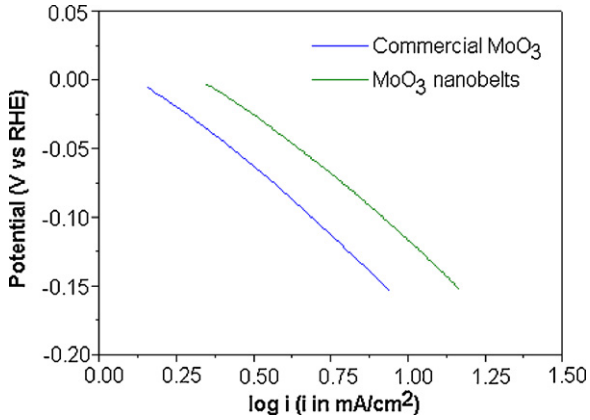

Fig. 7. Tafel plots of α-MoO_3 nanobelts and commercial MoO_3 microparticles.

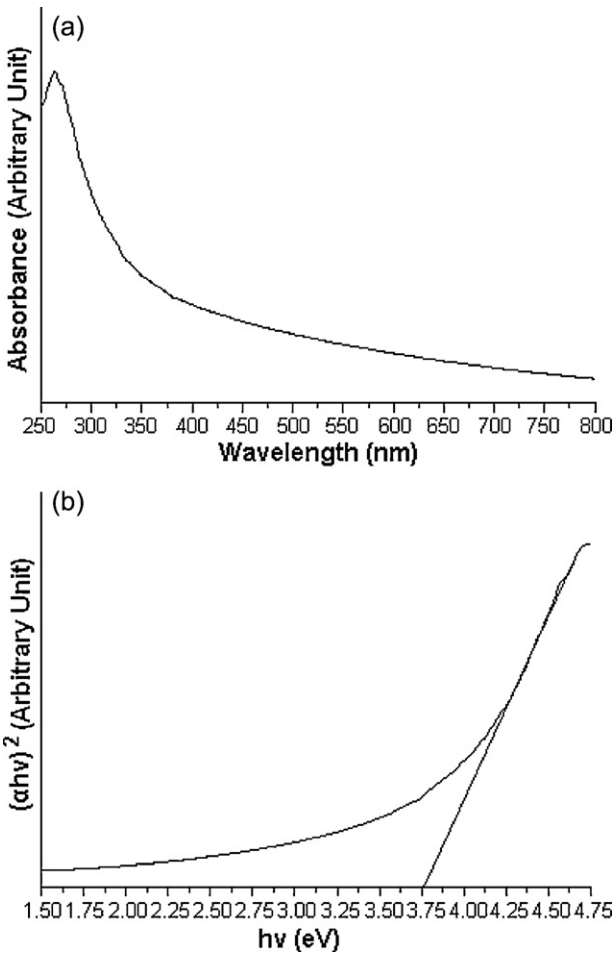

Fig. 8. (a) UV–vis absorbance, and (b) the $(\alpha h\nu)^2$ vs $h\nu$ plot of α-MoO_3 nanobelts.

and α-MoO_3 nanobelts, they showed the current density of −2.68, −4.89 and −8.33 mA/cm^2, and −4.54, −8.25 and −14.41 mA/cm^2 at −0.05, −0.10 and −0.15 V, respectively. The electrocatalytic activity of α-MoO_3 nanobelts is ~1.70 times higher than that of the commercial MoO_3 microparticles. (For interpretation of the references to color in this text, the reader is referred to the web version of this article.)

Tafel plots as shown in Fig. 7 were calculated from LSV data at low over-potential region from −0.005 to −0.035 V (vs RHE). Comparing Tafel plots between α-MoO_3 nanobelts (green/right) and commercial MoO_3 microparticles (blue/left), the exchange current density (I_o) of α-MoO_3 nanobelts (2.10 mA/cm^2) was higher than that of the commercial MoO_3 microparticles (1.34 mA/cm^2). The high exchange current density (I_o) of α-MoO_3 nanobelts implied that lower intrinsic electric resistance originated from the vectorial electron transfer along the crystal growth direction. This phenomenon has been apparently detected in 1-D nanostructure which preserved the high aspect ratio to their unique textural properties. Owing to the vectorial electron transfer, α-MoO_3 nanobelts could provide facile electron pathway, and the enhanced electrochemical activity was detected. Furthermore, the Tafel slope and onset potential of α-MoO_3 nanobelts were −131 mV/dec and +0.096 V vs RHE, respectively. They were higher than the −138 mV/dec and +0.094 V vs RHE of the commercial MoO_3 microparticles. More positive onset potential of α-MoO_3 nanobelts could turn out to be a more active electrocatalyst than the commercial MoO_3 microparticles. Lower Tafel slope has been related with the large number of electrons participating in HER. The number of electrons of α-MoO_3 nanobelts and commercial MoO_3 microparticles was 0.9 and 0.85, respectively. Consequently, these electrochemical results have provided that 1-D structured α-MoO_3 nanobelts as electrocatalyst could be a better performance than general 0-D particles for HER. The electrochemical data for HER was also summarized in Table 3. (For interpretation of the references to color in this text, the reader is referred to the web version of this article.)

3.4. Optical property of α-MoO_3 nanobelts

The optical absorption spectrum of α-MoO_3 nanobelts (Fig. 8a) exhibited the strong absorption centered at ~262 nm in the UV region, due to the charged transfer in the $[MoO_6]^{6-}$ octahedrons [29]. The direct band gap (E_g) was calculated from the relation between the absorption coefficient and photon energy given by

$$\alpha h\nu = (h\nu - E_g)^n \quad (8)$$

where α, h, ν, and E_g are the absorbance, Planck constant, photon frequency, and photonic band gap, respectively. The parameter n is a constant associated with the different types of electronic transition: $n = 1/2$, 2, 3/2 or 3 for direct allowed, indirect allowed, direct forbidden and indirect forbidden transitions, respectively [29–31]. Fig. 8b shows the plot of $(\alpha h\nu)^2$ vs $h\nu$. By extrapolating the linear portion of the curve to zero absorbance, the direct E_g of α-MoO_3 nanobelts was determined to be 3.75 eV, larger than that of its bulk state (2.9 eV) [32], due to the quantum size effect [33]. The gap is increased with the decrease in the particle sizes and increase in the surface area to volume ratios. Morphologies, crystalline degree and structural order–disorder can play the role in the gap [34] as

Table 3
Electrocatalytic HER properties of commercial MoO_3 microparticles and α-MoO_3 nanobelts.

Electrocatalyst	Specific activity at −0.05 V (mA/cm^2)	Specific activity at −0.10 V (mA/cm^2)	Specific activity at −0.15 V (mA/cm^2)	Onset potential (V vs RHE)	Tafel slope[a] (mV/dec)	I_o (mA/cm^2)
MoO_3 microparticles	−2.68	−4.89	−8.33	+0.094	−138	1.34
α-MoO_3 nanobelts	−4.54	−8.25	−14.41	+0.096	−131	2.10

[a] In the low overpotential region from −0.005 V to −0.035 V (vs RHE).

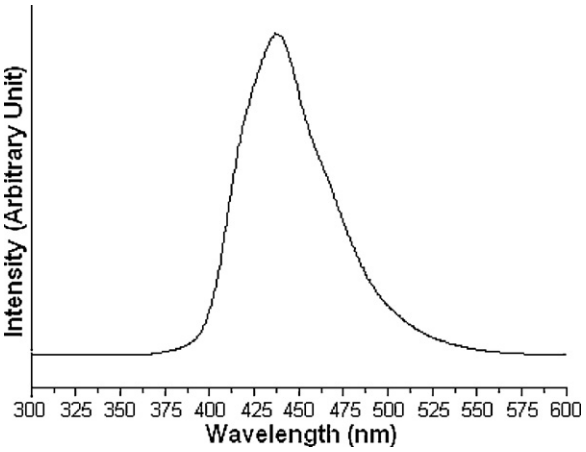

Fig. 9. PL emission of α-MoO_3 nanobelts at room temperature.

well. The direct allowed E_g for the absorbance of α-MoO_3 nanobelts was caused by the charged transition from the uppermost valence band of O_{2p} to the lowest conduction band of Mo_{4d} ($O_{2p} \rightarrow Mo_{4d}$) of α-$MoO_3$ [35].

Fig. 9 is a photoluminescence spectrum of α-MoO_3 nanobelts excited by 337 nm wavelength at room temperature. It shows a broad peak at 375–550 nm with the maximum emission peak at 437 nm, corresponding to the report of Song et al. [36], due to the charged transition from the lowest conduction band to the uppermost valence band of α-MoO_3 nanobelts.

4. Conclusions

In summary, α-MoO_3 nanobelts with >10 μm long and <200 nm wide were successfully synthesized under hydrothermal reaction at 180 °C for 20 h in controlling agent solution. In the present research, α-MoO_3 nanobelts grew along the *c* axis, with the ±(1 0 0) top and bottom and ±(0 1 0) side surfaces. Comparing HER of α-MoO_3 nanobelts and that of the commercial MoO_3 microparticles, the first showed the better performance electrochemical HER activity, including the 3.75 eV energy gap caused by the $O_{2p} \rightarrow Mo_{4d}$ charged transition, and the 437 nm emission peak excited by 337 nm wavelength at room temperature.

Acknowledgements

We wish to thank the National Nanotechnology Center (NANOTEC), National Science and Technology Development Agency, for providing financial support through the project code: P-10-11345, the Thailand's Office of the Higher Education Commission through the National Research University (NRU) Project, and the Thailand Research Fund (TRF) through the TRF Research Grant, including Graduate School of Chiang Mai University through the general support.

Appendix A. Supplementary data

Supplementary data associated with this article can be found, in the online version, at doi:10.1016/j.jallcom.2011.12.024.

References

[1] R.Q. Song, A.W. Xu, B. Deng, Y.P. Fang, J. Phys. Chem. B 109 (2005) 22758–22766.
[2] S.R. Dhage, M.S. Hassan, O.B. Yang, Mater. Chem. Phys. 114 (2009) 511–514.
[3] L. Mai, B. Hu, W. Chen, Y. Qi, Ch. Lao, R. Yang, Y. Dai, Zh.L. Wang, Adv. Mater. 19 (2007) 3712–3716.
[4] X.W. Lou, H.Ch. Zeng, Chem. Mater. 14 (2002) 4781–4789.
[5] G. Wei, W. Qin, D. Zhang, G. Wang, R.y. Kim, K. Zheng, L. Wang, J. Alloys Compd. 481 (2009) 417–421.
[6] A. Phuruangrat, D.J. Ham, S. Thongtem, J.S. Lee, Electrochem. Commun. 11 (2009) 1740–1743.
[7] G.S. Zakharova, C. Täschner, V.L. Volkov, I. Hellmann, R. Klingeler, A. Leonhardt, B. Büchner, Solid State Sci. 9 (2007) 1028–1032.
[8] J.H. Ryu, J.W. Yoon, K.B. Shim, Solid State Commun. 133 (2005) 657–661.
[9] S.S. Mahajan, S.H. Mujawar, P.S. Shinde, A.I. Inamdar, P.S. Patil, Sol. Energy Mater. Sol. Cells 93 (2009) 183–187.
[10] Sh. Wang, Y. Zhang, X. Ma, W. Wang, X. Li, Z. Zhang, Y. Qian, Solid State Commun. 136 (2005) 283–287.
[11] A. Phuruangrat, D.J. Ham, S.J. Hong, S. Thongtem, J.S. Lee, J. Mater. Chem. 20 (2010) 1683–1690.
[12] Powder Diffract. File, JCPDS-ICDD, 12 Campus Boulevard, Newtown Square, PA 19073-3273, U.S.A., 2001.
[13] Ch.V.S. Reddy, E.H. Walker Jr., S.A. Wicker Sr., Q.L. Williams, R.R. Kalluru, J. Solid State Electrochem. 13 (2009) 1945–1949.
[14] L. Cheng, M. Shao, X. Wang, H. Hu, Chem. Eur. J. 15 (2009) 2310–2316.
[15] M.B. Rahmani, S.H. Keshmiri, J. Yu, A.Z. Sadek, L. Al-Mashat, A. Moafi, K. Latham, Y.X. Li, W. Wlodarski, K. Kalantar-zadeh, Sens. Actuators B 145 (2010) 13–19.
[16] Ch.V.S. Reddy, E.H. Walker Jr., Ch. Wen, S. Mho, J. Power Sources 183 (2008) 330–333.
[17] V.M. Mohan, H. Bin, W. Chen, J. Solid State Electrochem. 14 (2010) 1769–1775.
[18] D. Liu, W.W. Lei, J. Hao, D.D. Liu, B.B. Liu, X. Wang, X.H. Chen, Q.L. Cui, G.T. Zou, J. Liu, S. Jiang, J. Appl. Phys. 105 (2009) 023513-1–023513-7.
[19] X. Chen, W. Lei, D. Liu, J. Hao, Q. Cui, G. Zou, J. Phys. Chem. C 113 (2009) 21582–21585.
[20] S. Phadungdhitidhada, P. Mangkorntong, S. Choopun, N. Mangkorntong, Ceram. Int. 34 (2008) 1121–1125.
[21] M. Dieterle, G. Weinberg, G. Mestl, Phys. Chem. Chem. Phys. 4 (2002) 812–821.
[22] T. Siciliano, A. Tepore, E. Filippo, G. Micocci, M. Tepore, Mater. Chem. Phys. 114 (2009) 687–691.
[23] L.G. Pereira, L.E.B. Soledade, J.M. Ferreira, S.J.G. Lima, V.J. Fernandes Jr., A.S. Araújo, C.A. Paskocimas, E. Longo, M.R.C. Santos, A.G. Souza, I.M.G. Santos, J. Alloys Compd. 459 (2008) 377–385.
[24] L. Seguin, M. Figlarz, R. Cavagnat, J.C. Lassègues, Spectrochim. Acta Part A 51 (1995) 1323–1344.
[25] T. Xia, Q. Li, X. Liu, J. Meng, X. Cao, J. Phys. Chem. B 110 (2006) 2006–2012.
[26] X.K. Hu, Y.T. Qian, Z.T. Song, J.R. Huang, R. Cao, J.Q. Xiao, Chem. Mater. 20 (2008) 1527–1533.
[27] L. Zheng, Y. Xu, D. Jin, Y. Xie, Chem. Mater. 21 (2009) 5681–5690.
[28] J. Chen, H. Yang, L. Chang, W. Fu, Y. Zeng, H. Zhu, G. Zou, Front. Phys. China 1 (2007) 92–95.
[29] Y. Keereeta, T. Thongtem, S. Thongtem, J. Alloys Compd. 509 (2011) 6689–6695.
[30] T. Thongtem, S. Jattukul, Ch. Pilapong, S. Thongtem, Curr. Appl. Phys. 12 (2012) 23–30.
[31] S. Suwanboon, R. Tanattha, R. Tanakorn, Songklanakarin J. Sci. Technol. 30 (2008) 65–69.
[32] Y. Zhao, J. Liu, Y. Zhou, Z. Zhang, Y. Xu, H. Naramoto, S. Yamamoto, J. Phys.: Condens. Matter 15 (2003) L547–L552.
[33] T. Thongtem, A. Phuruangrat, S. Thongtem, Appl. Surf. Sci. 254 (2008) 7581–7585.
[34] T. Thongtem, A. Phuruangrat, S. Thongtem, Mater. Lett. 61 (2007) 3235–3238.
[35] M. Itoh, K. Hayakawa, Sh. Oishi, J. Phys.: Condens. Matter 13 (2001) 6853–6864.
[36] J. Song, X. Ni, D. Zhang, H. Zheng, Solid State Sci. 8 (2006) 1164–1167.